THE EFFECT OF ANISOTROPIC SCATTER ON ATMOSPHERIC NEUTRON TRANSPORT

THESIS

MARCH 2015

Nicholas J. McIntee, Major, USA

AFIT-ENP-MS-15-M-085

DEPARTMENT OF THE AIR FORCE

AIR UNIVERSITY

AIR FORCE INSTITUTE OF TECHNOLOGY

Wright-Patterson Air Force Base, Ohio

AFIT-ENP-MS-15-M-085

THE EFFECT OF ANISOTROPIC SCATTER ON ATMOSPHERIC NEUTRON TRANSPORT

THESIS

Presented to the Faculty

Department of Engineering Physics

Graduate School of Engineering and Management

Air Force Institute of Technology

Air University

Air Education and Training Command

In Partial Fulfillment of the Requirements for the

Degree of Master of Science in Nuclear Engineering

Nicholas J. McIntee, BSE

Major, USA

March 2015

AFIT-ENP-MS-15-M-085

THE EFFECT OF ANISOTROPIC SCATTER ON ATMOSPHERIC NEUTRON TRANSPORT

Nicholas J. McIntee, BSE
Major, USA

Committee Membership:

Dr. Kirk A. Mathews
Chair

Dr. Justin Clinton
Member

LTC Stephen R. McHale
Member

Dr. David Gerts
Member

AFIT-ENP-MS-15-M-085

Abstract

Anisotropy is present in the angular distributions of neutrons departing from a nuclear scattering event. This anisotropy cannot be defined in a closed-form solution, as in the Klein-Nishina distribution for gamma rays following scattering events, nor is the degree and behavior of anisotropy only dependent on the incident energy of the particle. In fact, for neutrons leaving a scattering event, the anisotropic behavior of the angular distribution is dependent on the incident energy of the neutron, the type of scatter being elastic or inelastic along with the inelastic level, and the species struck.

The underlying question is, if anisotropic behavior is worth the computational cost to be included in certain simulations, and if so, what level of precision is effected by the inclusion of anisotropic scatter.

A Watt spectrum of U^{235} fission neutrons was examined as it collided with species in a nitrogen-oxygen atmosphere. In a stochastic manner, 10^8 collision samples were taken, utilizing cross section-based weighting for random sampling of collision types and cross section weighting along with concentration weighting to determine the species struck. The collective anisotropy of the resultant angular distribution was apparent, with a definite average forward bias across the spectrum and a bias toward scattering angles less than 30 degrees.

Additionally, when lower energies are eliminated from consideration, the forward bias increases. This leads to the conclusion that, on average, the higher the energy, the greater the apparent magnitude of the forward bias of the anisotropic scatter.

Using 1-D slab geometry, two studies were conducted exploring the relative effect of anisotropic scatter as compared to isotropic scatter in the center of mass reference frame. The maximum relative error of 0.24% was observed in the energy dimension and 0.23% in the time dimension. This can serve as a first approximation for more complex problem geometries and more robust scatter mechanics. In short, if precision is required past the second decimal place in long-distance high-altitude transport utilizing isotropic scatter in the center of mass reference frame, anisotropy in the center of mass reference frame deserves consideration.

Acknowledgments

I would like to express my sincere appreciation to my faculty advisor, Dr. Kirk Mathews, for his time and patience throughout the course of this thesis effort. His experience in modeling software techniques was indispensable. I would also like to thank my peers and colleagues for their support during this effort.

Nicholas J. McIntee

Table of Contents

List of Figures

List of Tables

THE EFFECT OF ANISOTROPIC SCATTER ON ATMOSPHERIC NEUTRON TRANSPORT

I. Introduction

In general, the response of any object or medium to neutron radiation depends on the properties of the object and energy of that particle. Any system's response also depends on the angle of incidence of the neutron. Combining the energy and angle of incidence, in the rest frame of the object or system of concern, dictates the response the system will have to that incident neutron. This object of concern might be a sensor of some type or particles in the medium subjected to or exposed to the neutron flux.

The response of a system can change based on the quantity of neutrons, not just the overall energy deposited by a neutron flux. More plainly, a small number of high energy neutrons as compared to a large number of low energy neutrons will generate different responses, even though the sum of energy might be the same.

Any model for this type of neutron transport will incorporate an energy range of interest, times of arrival of neutrons, and flux or fluence. Additionally, based on the problem parameters and available input data, a given model will have requirements for precision and accuracy. Some applications may tolerate large errors and others may need extremely precise calculations. This precision and accuracy requirement drives the level of fidelity required within a model.

Application

The Air Force Technical Applications Center (AFTAC) monitors compliance with nuclear test ban treaties. Reliability of the U.S. Nuclear-detonation Detection System (USNDS) requires observing multiple phenomenologies, including neutron radiation. AFIT is developing a new, more-capable Monte Carlo neutron radiation transport simulator in support of these efforts.

HASTE-N

High-Altitude and Space Transport Estimator – Neutrons or HASTE-N is a software package being developed by Dr. Kirk Mathews. HASTE-N, in general, is designed to simulate high fidelity, high altitude neutron transport using stochastic Monte-Carlo methods in an effort to generate accurate modeling for specific types of low-density medium transport problems. [1]

The cornerstone of HASTE-N, and why it is different than general purpose stochastic transport codes, is based on the inclusion of physical processes that are normally not included in neutral particle transport. One key process is the independent motion of the material in the problem, including the neutron source, the transport medium, and the object of interest itself. Typically these are all stationary, which is not the case in high altitudes with detectors in orbit. Another key process is the influence of gravity on the neutron. For most neutral particle transport problems in short time

scales or over small distances, gravity is not included. Finally, the thermal motion of atoms in the transport medium is considered in order to more accurately predict the energy of a neutron following a scatter. [2]

The HASTE-N code is also developed to take advantage of some of the special features of the problem set of long distance low-density medium transport, predominantly long distances between collisions, changing medium density, and gravitational effects. Properties of low density air as the medium and known gravitational parameters allow optimization of the code for tasks like cross-section lookup, mean free path calculations, root-solving problems.

Additionally, HASTE-N allows the user to toggle the inclusion of different physical processes independently. This permits individual processes to be examined for verification purposes both during development and by end users. An individual process can then be studied for its net effect on a given problem. The added benefit of this feature is the ability to trade fidelity for execution speed when required.

HASTE-N-TE

HASTE-N Test Environment (HASTE-N-TE) is a software package developed by Captain Whitman Daily to provide a simulation environment for the testing of HASTE-N modules separate from the complexity of the overall HASTE-N software package.

For this reason, HASTE-N-TE functions as the environment used to test the modules discussed in this document.

Development Focus

The underlying question is if anisotropic behavior is worth the computational cost to be included in certain HASTE-N problem runs, and if so, what level of precision is effected by the inclusion of anisotropic scatter. In order to address this question, first anisotropic scatter was implemented, then verified, and finally, the measurement of the net effect on an overall simulation.

The focus of this document is on the development of a small part of the HASTE-N software package as a whole, namely the modules covering scatter mechanics and cross-section look ups. The effort described here was to implement and verify these portions of HASTE-N individually to contribute to the verification of the software package as a whole.

The first module covers the anisotropic scatter of neutrons following a scattering interaction with a species of nuclei in the air. In general, implementation of anisotropic behavior consists of interpreting and interpolating Legendre polynomial coefficients from ENDF files, constructing probability density functions and cumulative distribution functions from interpolated coefficients, and evaluating the angular distribution to determine scattering angle.

The second module is focused on the ingestion and use of cross-section data from ENDF file extractions. These cross sections along with atmospheric composition data are used by HASTE-N to determine the species struck, mean free path length, the type of interaction, and the inelastic level of scattering events. Additionally, because cross-sections are used so frequently during calculations of each particle history, emphasis was placed on execution speed of cross-section look ups.

Verification

Following the implementation and testing of the anisotropic scatter and cross-section modules, a stripped down version of HASTE-N referred to as HASTE-N Test Environment (HASTE-N-TE) developed by Capt. Whitman Daily was used to verify and test the behavior of the two modules. Additionally, parameter studies were conducted to observe the effect of anisotropy on long distance high altitude transport problems as simulated by HASTE-N-TE.

II. Theory

The Anisotropic Scatter of Neutrons

Following collision with a nucleus, an elastic or inelastic collision, the neutron departs the nucleus with a given deflection angle from the initial direction of travel. This angular distribution is uniform about the initial direction of travel of the neutron, but the deviation from that initial direction is drawn from a probability distribution function and varies from 0 to π radians (or 0 to 180 degrees).

Consider a neutron, initially travelling in direction $\hat{\Omega}' = \vec{v}'/v'$, that collides with a nucleus and leaves the collision in a new direction $\hat{\Omega}$. The cosine of the deflection angle for the collision is usually denoted as $\mu_0 = \hat{\Omega}' \cdot \hat{\Omega}$. This is the cosine of a polar angle for spherical coordinates with the pole aligned with $\hat{\Omega}'$. The other spherical coordinate angle, representing rotation around that axis is conventionally denoted as ω_0. For isotropic scattering, μ_0 is be uniformly distributed between -1 (backscatter) and +1 (forward scatter), and ω_0 is uniformly distributed between $-\pi$ and π. The subscript zero is dropped for conciseness of notation in the rest of this thesis.

The classical mechanics solution for the scattering collision of two spheres is that the distribution in isotropic in the center of mass (CM) frame. Thus, the probability density function (PDF) is

$$f_{isotropic}\left(\mu\right)=\begin{cases}1/2 & -1\le\mu\le+1\\ 0 & else\end{cases}$$
$$f_{isotropic}\left(\omega\right)=\begin{cases}1/2\pi & -\pi<\omega\le+\pi\\ 0 & else\end{cases}. \qquad [2.1]$$

Using this classical approximation, if the mass of the nucleus is much greater than that of a neutron, such as for neutron scattering in Uranium, it suffices for many applications to approximate the angular distribution as isotropic in the lab frame. However, in scattering a neutron from an atom of air, the mass ratio is from about 14:1 for nitrogen-14 to about 18:1 for oxygen 18. In these cases, isotropic in the lab frame is not an acceptable approximation to isotropic scatter in the CM frame. The relation between the scattering cosine in the lab frame and in the CM frame for elastic scatter, is simply

$$\mu_{CM}=\frac{-1+{\mu_{lab}}^2+\mu_{lab}\sqrt{-1+A^2+{\mu_{lab}}^2}}{A}, \qquad [2.2]$$

where A is the ratio of the mass of the nucleus to that of the neutron. For elastic scatter with $A>1$, the PDF in the lab frame is

$$f_{lab}\left(\mu\right)=f_{CM}\left(\mu_{cm}\right)\frac{\left(\mu_{lab}+\sqrt{-1+A^2+{\mu_{lab}}^2}\right)^2}{2A\sqrt{-1+A^2+{\mu_{lab}}^2}}. \qquad [2.3]$$

A Cartesian plot of the PDF for isotropic scatter, for A=14 and A=18, is presented in figure 1.

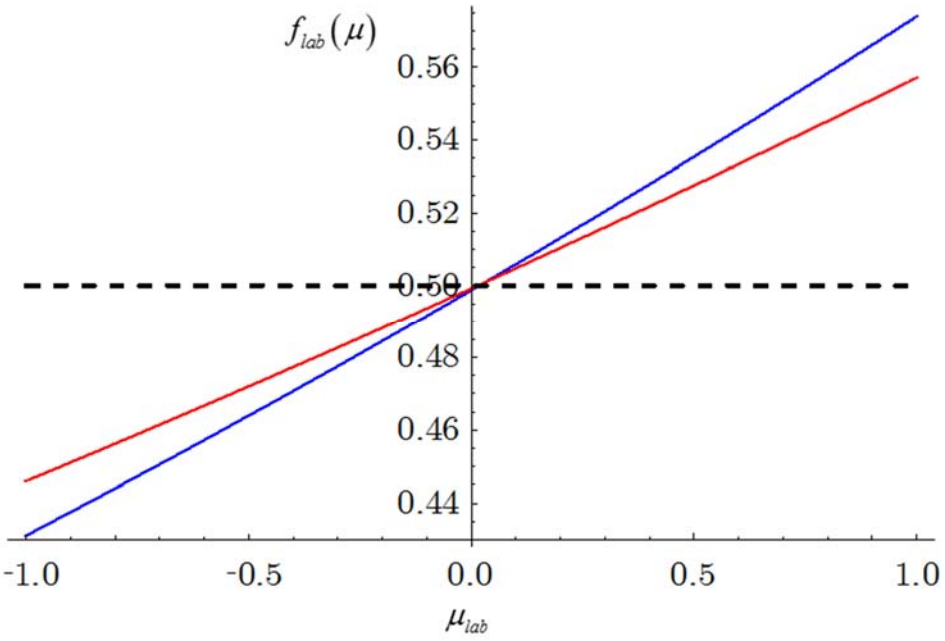

Figure 1: Probability density function for isotropic scatter in the lab frame, plotted in Cartesian coordinates. Curves are displayed for A=14, A=18, and A=∞.

The steeper curve (blue) is the PDF for the less massive atom, $A = 14$. The red curve is for $A = 18$. The dashed line is the PDF if scattering were isotropic in the lab frame, i.e., for $A = \infty$. It is easier to visualize the extent of the anisotropy using a plot of the surface of the distribution function $f\left(\mu\left(\theta\right),\omega\right)$. Figure 2 shows this function for a neutron that was initially moving directly to the right. Thus, the pole on the right of the not-quite-sphere is forward scatter and the one on the left is backscatter.

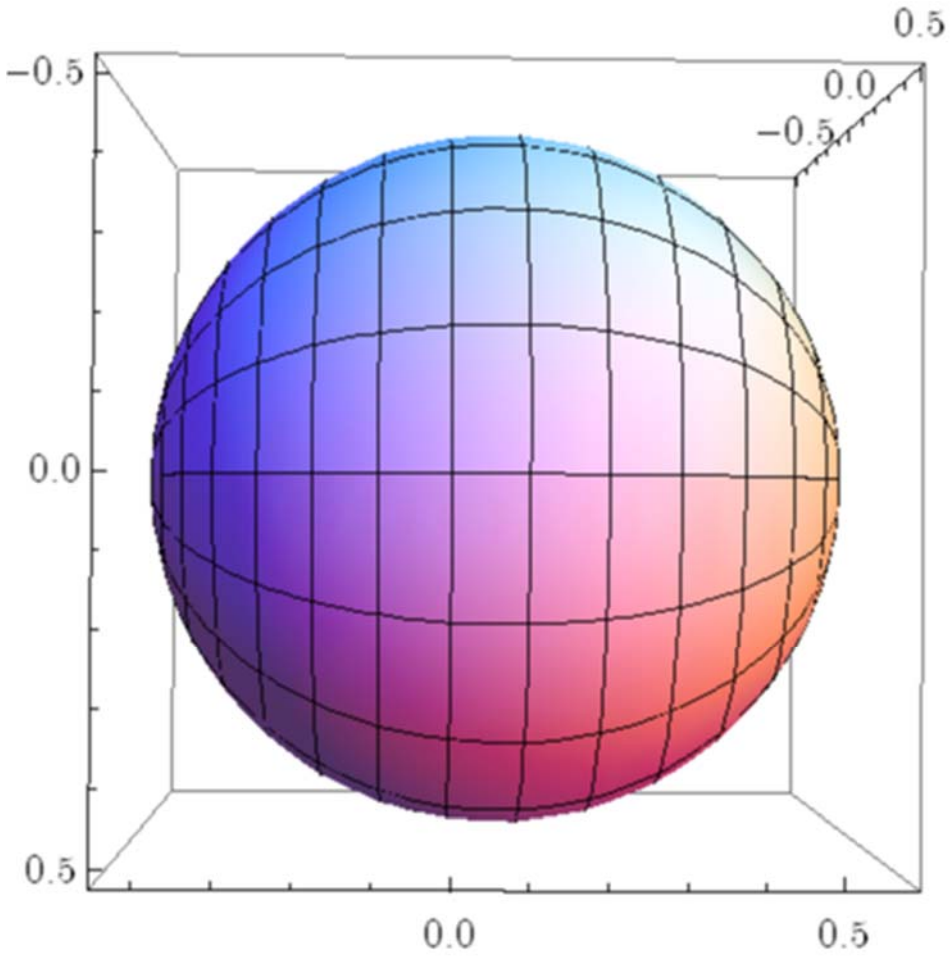

Figure 2: A plot of the surface of the distribution function $f(\mu(\theta),\omega)$ for a neutron incident from the left moving right. Note the plot is rotationally symmetric about the direction of travel of the incident neutron.

However, these plots are always rotationally symmetric around the axis, so one usually finds plots that are a cross-section of this shape where it intersects with a plane through the origin perpendicular to the line of sight. Such a plot is a polar parametric plot with μ as the independent variable, $f\left(\mu\right)$ as the radius and angular coordinate $\theta = \arctan\left(\mu\right)$. Figure 3 presents the distributions from figure 2 in this way. Forward

scatter is for $\mu = 1$, whence $\theta = 0$, which is to the right in figure 3. Sideways scatter is for $\mu = 0$, whence $\theta = \pi / 2$. This plot makes it easy to see the extent of anisotropy. Remember that this is a plot of the PDF of μ, not the PDF of θ.

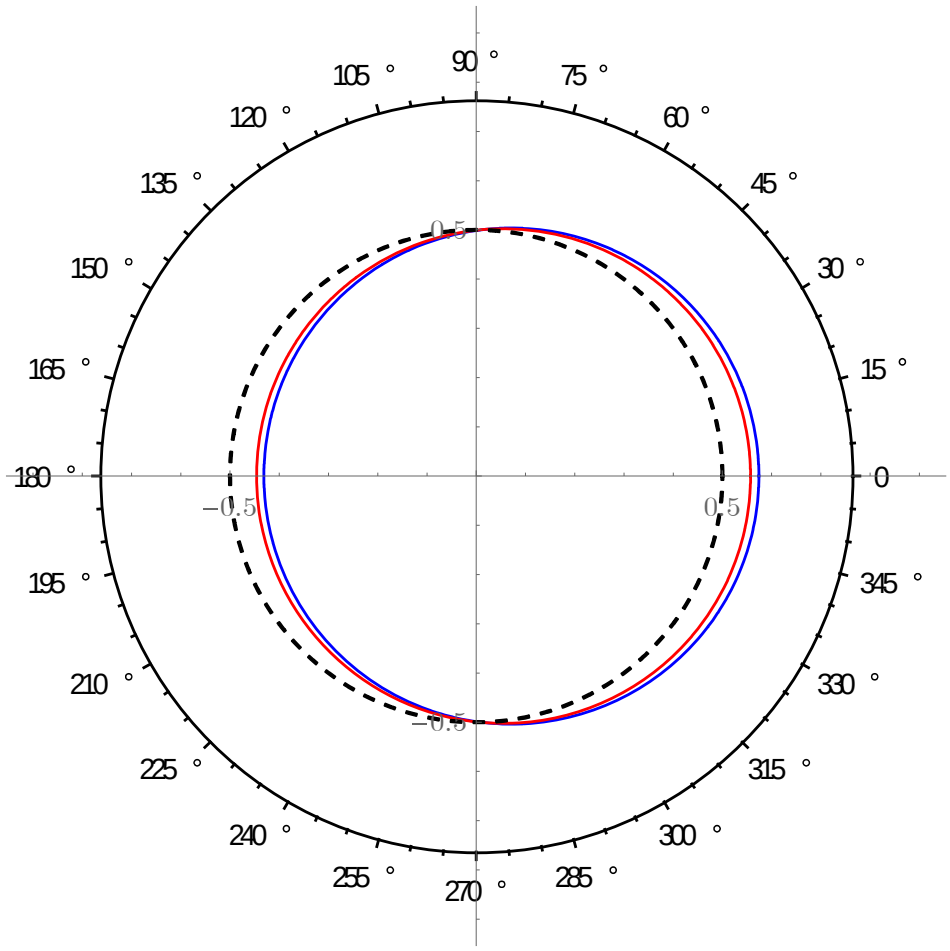

Figure 3: A polar parametric plot with μ as the independent variable, $f(\mu)$ as the radius and angular coordinate $\theta = \arctan(\mu)$. Curves are displayed for A=14, A=18, and A=∞.

This type of angular distribution is commonly encountered in the content of photons deflecting off free electrons, resulting in the Klein-Nishina formula. In the case

of photons colliding with electrons, this distribution is only dependent on the initial energy and is well-defined in a closed-form equation.

The remainder of this thesis examines the extent to which scattering in the CM frame is not actually isotropic (due to quantum-mechanical effects). In all subsequent formulas and plots, μ denotes the scattering deflection cosine *in the center of mass frame*.

The actual anisotropic angular distribution of neutrons (in the CM frame) following a collision with a nucleus, is dependent on the initial energy of the collision in the center of mass, the species of nucleus struck (both atomic number and weight), and the excited level of the nucleus as a result of an inelastic collision. Unfortunately, there is no known closed form solution for this angular distribution. Experimentally, these distributions are measured. ENDF presents coefficients for truncated Legendre polynomial series that are used to approximate the distribution functions in the form

$$f\left(\mu\right) = \sum_{j=0}^{n} \frac{2j+1}{2} \sigma_j P_j\left(\mu\right). \qquad [2.4]$$

Legendre Polynomials

Legendre polynomials, in general, are azimuthally symmetric solutions to Legendre's differential equation,

$$\frac{d}{dx}\left[\left(1-x^2\right)\frac{d}{dx}P_n\left(x\right)\right]+n\left(n+1\right)P_n\left(x\right)=0 \qquad [2.5]$$

where $P_n\left(x\right)$ is the n^{th} Legendre polynomial. Solving the above ordinary differential equation is not related to the approximation of an angular distribution function, but the fact that the polynomial solutions to the ODE are orthogonal to each other makes these polynomials ideal for the estimation of a function that does not have a closed form; the use of additional polynomials from the generated series allows achievement of the desired precision of the estimator function.

The Legendre polynomials from n=0 to n=5 are as follows:

$$\begin{aligned}
P_0\left(x\right) &= 1 \\
P_1\left(x\right) &= x \\
P_2\left(x\right) &= {}^{1}\!\!\diagup\!\!_{2}\left(3x^2-1\right) \\
P_3\left(x\right) &= {}^{1}\!\!\diagup\!\!_{2}\left(5x^3-3x\right) \\
P_4\left(x\right) &= {}^{1}\!\!\diagup\!\!_{8}\left(35x^4-30x^2+3\right) \\
P_5\left(x\right) &= {}^{1}\!\!\diagup\!\!_{8}\left(63x^5-70x^3+15x\right)
\end{aligned} \qquad [2.6]$$

The polynomials from equation [2.6] are shown graphically in Figure 4 below.

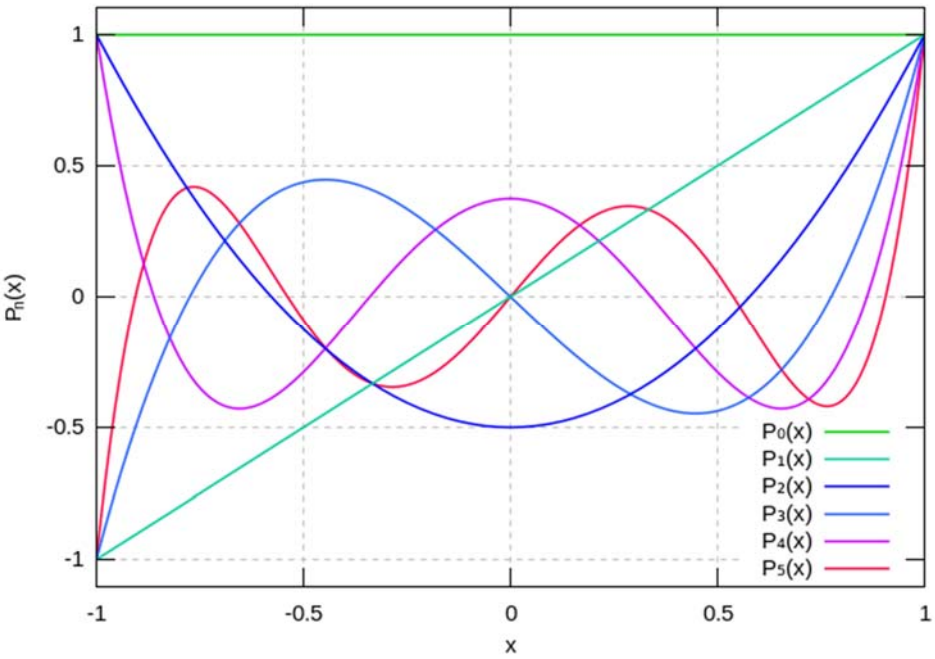

Figure 4: Graph of the First Five Legendre Polynomials. The polynomials are shown on the interval ranging (-1,1) and are shown absent any weighting coefficients. (http://en.wikipedia.org/wiki/Legendre_polynomials)

Legendre Polynomial Generation

The Legendre polynomials are typically defined and generated recursively using Bonnet's recursion formula:

$$\begin{aligned} P_0\left(x\right) &= 1 \\ P_1\left(x\right) &= x \\ P_n\left(x\right) &= \frac{(2n-1)x\mathrm{P}_{n-1}(x)-(n-1)\mathrm{P}_{n-2}(x)}{n} \end{aligned} \qquad [2.7]$$

Though able to be generated through recursion and expanded into single polynomials as in equation [2.6], the polynomials can be evaluated during the recursion, resulting in less possibility of computational error due to repeated arithmetic operations.

Using Legendre Polynomials

These polynomials are used here as an estimator of f(μ), the probability density function (PDF) of the cosine of the scattering angle of a neutron and nucleus collision. The polynomials, individually weighted and summed together, form the function estimator, $f\left(\mu\right)$. [3]

$$f\left(\mu\right) = \begin{cases} \sum_{j=0}^{n} a_j P_j(\mu) & -1 \le \mu \le 1 \\ 0 & else \end{cases}. \qquad [2.8]$$

where

$$a_j = \left(\frac{2j+1}{2}\right)\sigma_j \qquad [2.9]$$

and the σ_j coefficients are tabulated in ENDF. To save execution time in the Monte Carlo code, the coefficients a_j are computed and stored in arrays as the coefficients σ_j are read in from the ENDF files.

The factor $\frac{2j+1}{2}$ arises in the orthogonalization of the Legendre polynomials:

$$\int_{-1}^{1} \frac{2j+1}{2} P_j\left(\mu\right) P_k\left(\mu\right) d\mu = \delta_{j,k} = \begin{cases} 1 & j = k \\ 0 & j \neq k \end{cases} . \qquad [2.10]$$

A PDF is not only normalized to integrate to 1, but also must be non-negative everywhere. The former is guaranteed for $a_0 = 1/2$; the latter depends on the values of the remaining coefficients. Presuming non-negativity, it can be integrated to produce the CDF,

$$F\left(\mu\right) = \int_{-1}^{\mu} f\left(\mu'\right) d\mu' , \qquad [2.11]$$

which must be monotone non-decreasing.

Cumulative Distribution Function Evaluation

In order to retrieve a useful value from the PDF in equation [2.8], as in the chance that a neutron scatters in a specific direction range, the PDF must be integrated for use as a CDF. The CDF is

$$F\left(\mu\right) = \int_{-1}^{\mu} \tilde{f}\left(x\right) dx = \sum_{j=0}^{n} a_j \int_{-1}^{\mu} P_j\left(x\right) dx = \sum_{j=0}^{n+1} b_j P_j\left(\mu\right) \qquad [2.12]$$

where the coefficients b_j are given by

$$b_j = \begin{cases} c_0 - c_1 & j = 0 \\ c_{j-1} - c_{j+1} & j = 1,..,n-1 \\ c_{j-1} & j = n, n+1 \end{cases} \qquad [2.13]$$

with

$$c_j = \frac{a_j}{2j+1} \qquad [2.14]$$

Like the PDF, the CDF can be generated and evaluated recursively. This is done for two reasons, the first for the minimizing of arithmetic error propagation and the second for an increase in execution speed.

Neutron Cross Sections

In general, a cross section governs the probability that a given interaction can occur. In the context here, the probability that an incident neutron will interact with a nucleus, sometimes referred to as total cross section for interaction, σ_{total}. Several interactions of a neutron with a nucleus can occur, including absorption, elastic scatter (n,n), inelastic scatter (n,n'), and other less common types.

Cross Section for Air

Cross section data is readily available for dry air at sea level at standard temperature and pressure and is well-supported by experimental data. For use in HASTE-N, this data would not accurately depict the problem, since the software is designed to define the atmosphere's composition for each problem. A more consistent

approach is to use the defined atmosphere to construct a total cross section for the defined atmosphere.

For example, for total cross section for interaction for air, $\sigma_{total(air)}$,

$$\begin{aligned}\sigma_{total(\text{air})} &= \sum_{k=1}^{l} f_k^{isotope,air}\sigma_{total(\text{isotope } k)} \\ &= \sum_{i=1}^{n}\sum_{j=1}^{m_i} f_i^{element,air} f_j^{isotope,element}\sigma_{total(\text{element } i,\text{isotope } j)}\end{aligned} \qquad [2.15]$$

where l is the total number of species in the atmosphere, n is the number of elements in the atmosphere, m_i is the number of isotopes of element i, $f_k^{isotope,air}$ is the atmospheric fraction of isotope k, and so on.

Based upon how the atmospheric concentrations are specified, $\sigma_{total(air)}$ can be constructed in two ways, both displayed in equation [2.15]. If each species to be considered in the atmosphere (elements or isotopes) is listed along with the fraction of the air it comprises, the cross sections of each species, weighted by their atmospheric fraction (f_k) are summed to produce the total cross section. If the atmosphere is instead further specified by the fraction of component elements (f_i), along with the fraction of occurrence of isotopes of that element (f_j), the cross sections of each species is weighted by both the elemental composition of the atmosphere along with the natural occurrence of the isotopes of that element, then summed to produce the total cross section.

This total cross section for interaction for air can then be used for mean free path calculations within HASTE-N

The Watt Spectrum

To define any fission spectrum in the Evaluated Nuclear Data Library, ENDL [4], the Watt spectrum can be used,

$$\mathrm{W}\left(a,b,E\right) = C\,\mathrm{e}^{-aE}\sinh\left(\sqrt{bE}\right) \qquad [2.16]$$

where E is the energy of the emitted neutron and the normalization constant, C, is obtained by integration of W:

$$C = \frac{1}{\int_0^\infty e^{-aE}\sinh\left(\sqrt{bE}\right)dE} = a\sqrt{\frac{4a}{\pi b}}\;e^{-\frac{b}{4a}} \qquad [2.17]$$

The coefficients a and b are different for each individual isotope as well as slight variances based on incident neutron energy.

To approximate the neutron fission spectrum for U^{235} as caused by neutrons in the MeV range, $a = 0.7\ \mathrm{MeV}^{-1}$ and $b = 1.0\ \mathrm{MeV}^{-1}$. [5] This is not a perfect approximation for the produced neutron spectrum of U^{235}, but will be used as a reasonable baseline for the purposes of parameter studies in this document. Further

details on use of the Watt spectra for fission spectra can be found in UCRL-TR-203351.

[4] (Note: That report contains an incorrect formula for the normalization constant.)

III. Methodology

Since HASTE-N is being developed in Fortran, the same development environment was selected for implementation of the scatter angle distribution and cross section modules. The functions and subroutines were written to interface with the existing development effort, and utilized existing routines from other HASTE-N modules. Microsoft Visual Studio 2013 along with the Intel Math Kernel Library was used to develop, debug, and test the modules.

Angular Distribution Implementation

Since the departure angle of a neutron following a scatter event is dependent on not just the species of nuclei struck and the incident energy of the neutron in the center of mass frame, but also on the type of scatter (elastic or inelastic), a large data set of Legendre coefficients is required for each isotope. For each isotope, the ENDF database has varying energy levels for elastic collisions as well as varying energy levels for the first thirty inelastic levels. One of the design parameters of this module was not to use a proprietary data file format; files directly from ENDF can be read by the software without alteration, allowing HASTE-N to be updated simply by adding newer ENDF files as they are released.

Legendre Coefficient Data

Dynamically sized, multidimensional data structures were constructed to hold the Legendre coefficients. Conceptually, the data is organized in a four dimensional matrix by isotope, energy, inelastic level, and the Legendre coefficient subscript. At the time of ingestion of the ENDF files, every one of those four dimensions must be determined dynamically.

The number of isotopes is based on the complexity of the atmosphere for a given problem. Elemental composition of the atmosphere as well as isotopes of each element are considered, based on the level of detail required for the atmosphere's composition in a specific problem. As a reasonable first approximation, the initial atmospheric composition was selected to contain the five most common species, in order of commonality: N^{14}, N^{15}, O^{16}, O^{18}, and O^{17}. The fraction of each element can be specified as well as the fraction of each isomer of each element in problem parameters.

In a given ENDF file containing Legendre Coefficients, coefficients for multiple incident energies are listed. The number of energies listed is primarily dependent on how much data was gathered experimentally. [6] For elastic collisions, the listed incident energies are from as low as $\sim 1.0 \times 10^{-5}$ eV and can range into the GeV level depending on the measurements recorded. For the inelastic level data, the lowest energy listed is the excitation energy for that inelastic excitation level, or the Q. For the purposes of

this software, the incident energy data extends no higher than 14.5 MeV, but this can be raised, provided the provided ENDF data extends to the desired energy level bound.

ENDF provides data for elastic collisions and for the first thirty inelastic levels of most isotopes, then a continuum for the levels above thirty. Fortunately, with the upper bound for energy set at 14.5 MeV, only the inelastic levels with Q values less than the upper energy bound need be considered. The software dynamically determines the levels required for each isotope based on the specified maximum incident energy.

The four-dimensional Legendre data structure contains the Legendre coefficients themselves. Based on the experimental data collected and the degree of anisotropy present for a given isotope, energy, and inelastic level combination, anywhere from 2 to 32 coefficients may be provided for energies below the upper energy bound of 14.5 MeV. [6] More than 32 coefficients may be provided for higher energies, and the software can easily be modified for this application if desired. It should be noted that larger magnitudes and greater numbers of coefficients indicate a more intense anisotropy of the selected scatter and hence a more complex function describing that distribution.

Once the collision type (isotope, energy, and inelastic level) has been fully determined through weighted random sampling, a linear interpolation of the coefficients from the energy above and below the target energy produces the coefficients used for the PDF and the CDF.

Cross Section Implementation

Once a collision location has been determined using mean free path calculations, cross sections of all the possible collision types are used to determine the species struck and the collision type. During this weighted random sampling, certain collision types can be suppressed, such as absorption or less common interactions like (n,2n) reactions. To determine the collision type, two weighted random samples must be executed; the first sampling selects the species struck and the second sampling determines the type of scattering event (elastic or inelastic) and the inelastic level.

To determine the species struck, total cross sections for each species in the atmosphere, weighted by the atmospheric fraction of each species, need to be considered. Additionally, in order to utilize embedded random number generators in the Math Kernel Library without additional mathematical operations, the random sample has been constructed to utilize random numbers on their intrinsic range, $\mathrm{R} \in [0,1)$.

The test used to select the struck species is

$$\mathrm{R} \leq \frac{\sum_{i=1}^{k} f_i \sigma_i^{total}}{\sum_{i=1}^{n} f_i \sigma_i^{total}} \qquad [3.1]$$

where R is a pseudo-random number, σ_i^{total} is the total cross section for interaction for the i^{th} species in the atmosphere and f_i is the fraction of the atmosphere represented by the i^{th} species, and n is the total number of species in the atmosphere. The test begins with k=1 and is repeated with the same random number, incrementing k until the test returns true or k=n-1. If the test is true, the k^{th} isotope is struck, and if k=n-1 the n^{th} isotope is known to be struck without performing the final test. To minimize the number of arithmetic operations, in successive tests, results from the previous summations can be used, as well as ordering the list of species with the highest atmospheric concentrations first

Once the species struck has been determined, the type of scatter (elastic or inelastic with level) must be determined. First, the maximum inelastic level is selected by comparing the energy of the incident neutron in the inertial frame of the struck nucleus to the excitation energies (Q) of the available inelastic levels. Any level with a Q greater than the incident energy (in the frame of the center of mass of the collision) cannot be reached and is therefor excluded. In a similar manner to equation [3.1], the level selection test is

$$\mathrm{R} \leq \frac{\sum_{i=0}^{k} \sigma_i^{scatter}}{\sum_{i=0}^{n} \sigma_i^{scatter}} \qquad [3.2]$$

where $\sigma_i^{scatter}$ is the cross section for scatter and excitation to the i^{th} inelastic level with i=0 being elastic, and n is the total number of available inelastic levels based on the Q value. The test begins with k=0 (elastic scatter) and is repeated with the same random number, incrementing k until the test returns true or k=n-1. If the test is true, the scatter is the k^{th} inelastic level, and if k=n-1 the scatter takes place at the n^{th} inelastic level, the highest level possible for that incident neutron energy without performing the final test. The summations occur during each iteration of the test, but summation results from previous iterations can be used to minimize arithmetic operations. In all examined cases, for all energies under 14.5 MeV, the elastic cross section is greatest, and hence the most likely scatter is elastic. In that elastic case, only one test occurs. Even though this test is O(n), functionally it is much faster due to the frequency of elastic scatter.

Unified energy grid

Since so many cross section lookups are required to fully define one particle's history, including mean free path calculations in air and multiple collision calculations as in equations [3.1] and [3.2], a unified energy grid is created prior to running a problem set in an effort to speed up individual cross section look ups.

In a given ENDF cross section file, the energies are not standardized across the whole ENDF library, but are based on round numbers (like 1.0e5 eV or 3.5e-6 eV) and

on excitation energy levels for the particular species being measured. Consequently, each ENDF cross section file has cross sections for a different set of energies.

The unified energy grid is a three dimensional matrix; the first dimension is energy, the second is the cross section type, and the third is the species or isotope. Much like the Legendre coefficient data, the size of two of these three dimensions must be determined dynamically, based on the problem definition and the contents of the ENDF libraries being used.

To construct the size of the first dimension, every energy listed in every ENDF file for the defined atmosphere is read in and placed in a list. Duplicates are eliminated from the list, and the list is sorted and truncated based on upper and lower energy bounds. This incorporates all the energies of interest for all of the isotopes taken into consideration.

The cross section types included as the second dimension are the cross section for elastic scatter, the cross section for total inelastic scatter, and the total cross section for interaction. Finally the third dimension is comprised of all the species included in the defined atmosphere.

Once the dimensions of the grid are determined, the cross sections themselves need to be populated into the unified grid. Some energy / cross section pairs directly map to the ENDF files, but some pairs in the grid will not directly map to the provided

data and need to be interpolated. Linear interpolation is used to avoid introducing arithmetic precision errors, as multiple linear interpolations are mathematically equivalent to a single linear interpolation. This is not the case with some other interpolation methods.

Once the grid is constructed, look ups into the grid will frequently not land on an energy boundary and will require interpolation, also linear. So, the cross section value used for interpolation may be interpolated twice, once when the unified grid is populated, and once when a table look up occurs. Since linear interpolating twice to a value is equivalent to linear interpolating once to the same value, no interpolation error is introduced.

Linear Interpolation

Given a standard linear interpolation of a function $f(x)$ with known values at x_0 and x_1,

$$f\left(x\right) = f\left(x_0\right) + \left(f\left(x_1\right) - f\left(x_0\right)\right)\left(\frac{x - x_0}{x_1 - x_0}\right) \qquad [3.3]$$

If another interpolated point, x', is calculated in the same interval,

$$f\left(x'\right) = f\left(x_0\right) + \left(f\left(x_1\right) - f\left(x_0\right)\right)\left(\frac{x' - x_0}{x_1 - x_0}\right) \qquad [3.4]$$

it can be shown that x can be found by interpolating x' with either x_0 or x_1.

$$f\left(x\right) = f\left(x_0\right) + \left(f\left(x'\right) - f\left(x_0\right)\right)\left(\frac{x - x_0}{x' - x_0}\right) \quad [3.5]$$

By substituting equation [3.4] into equation [3.5],

$$\begin{aligned} f\left(x\right) &= f\left(x_0\right) + \left(f\left(x_0\right) + \left(f\left(x_1\right) - f\left(x_0\right)\right)\left(\frac{x' - x_0}{x_1 - x_0}\right) - f\left(x_0\right)\right)\left(\frac{x - x_0}{x' - x_0}\right) \\ f\left(x\right) &= f\left(x_0\right) + \left(f\left(x_1\right) - f\left(x_0\right)\right)\left(\frac{x' - x_0}{x_1 - x_0}\right)\left(\frac{x - x_0}{x' - x_0}\right) \\ f\left(x\right) &= f\left(x_0\right) + \left(f\left(x_1\right) - f\left(x_0\right)\right)\left(\frac{x - x_0}{x_1 - x_0}\right) \end{aligned} \quad [3.6]$$

equation [3.3] is produced, showing multiple linear interpolations are mathematically equivalent to a single linear interpolation.

Verification Design

As with most program development efforts, the developed modules are tested independently from the larger programming effort, in order to focus the search for compilation, run time, and logic errors in the code. The majority of the verification work was performed in Microsoft Visual Studio 2013 [7] and graphical verification was performed in Matlab 2014b [8].

Anisotropy Testing

The first question to be addressed with regards to anisotropic behavior of neutrons following scattering events is, to what degree is anisotropic behavior present even in the simplest of conditions? With the provided ENDF data, prior to any simulation effort, the anisotropic angular distribution for the considered species was examined to determine if the anisotropic behavior was evident at all.

Collision Testing

With the use of the Watt spectrum for neutrons produced from the fission of U^{235} along with the atmospheric concentrations specified for a five species atmosphere (N^{14}, N^{15}, O^{16}, O^{18}, and O^{17}), the collision choosing functionality was tested. This serves not only to ensure all possible collision types were represented and functioning correctly, but also serves as an indicator of the general likelihood of individual scatter events occurring during a more expansive simulation.

Net Effect of Anisotropy

Finally, as an examination of the effect of anisotropy of neutron scatter on problems of this type, two parameter studies were conducted using HASTE-N-TE, incorporating atmospheric species concentrations, weighted scattering occurrence rates, and energies generated by a line source. Both of these studies utilized a flat-earth, stationary atmosphere model varying altitude and energy respectively.

IV. Results and Analysis

A Matlab 2014b script was written to construct the PDF from Legendre weighting coefficients combined with their associated polynomials and to plot them as in figure 3. Because the incident particles here have mass, the energy is in the center of mass frame of the collision, and may differ from the energy of the incident neutron in the lab reference frame based on the movement of the nucleus being struck.

Anisotropic Angular Distributions

Prior to examination of any results from simulations, the first step was to examine the anisotropic behavior of neutrons in general, using coefficients directly from ENDF, to determine any patterns or common behavior of the angular distributions in general. Note: The areas under different PDFs plotted as in figure 1 are all equal to 1, by the normalization of a PDF. However, the areas inside of different PDFs on parametric polar plots, as in figure 3 and in this chapter, are not related to normalization and can be very different.

First, the behavior of the angular distribution of a neutron in the exit channel following an elastic collision was considered. The isotope was fixed, and only energy was varied. The first isotope examined in this manner was O^{16}, and energy levels of 1 MeV, 4 MeV, and 7 MeV are shown in figure 5 below.

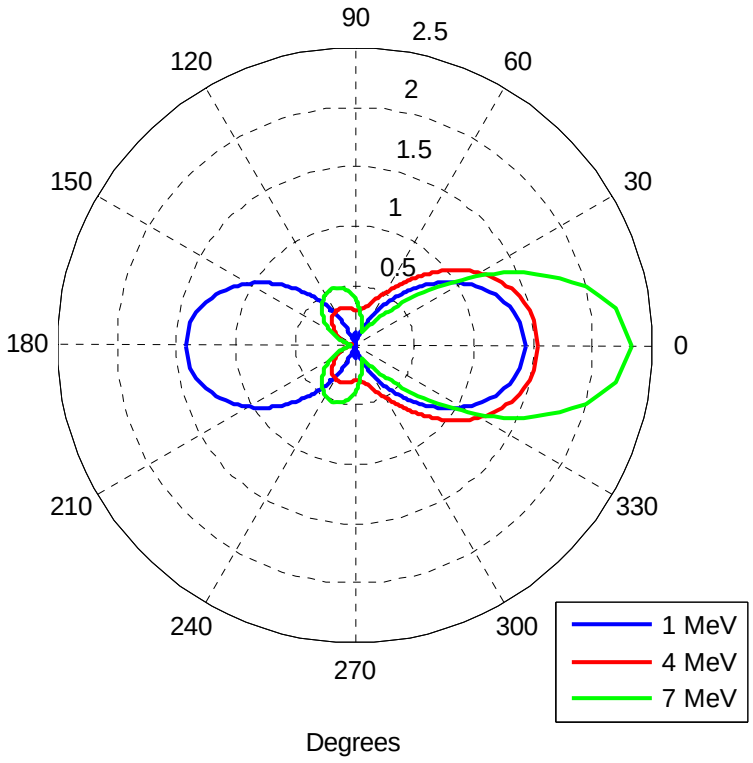

Figure 5: $f(\mu_{CM})$ plotted radially against $\theta(\mu_{CM})$ of Neutrons at 1 MeV, 4 MeV, and 7 MeV following elastic scattering events with O^{16}. These energies are measured in the reference frame of the center of mass of the collision. With changing energies of incident neutron colliding with the same species in only elastic scattering events, significantly different angular distributions result.

Knowing that isotropic behavior would be displayed as a circle of radius 0.5, anisotropic scatter is clearly present, as seen by two distinct lobes in the 1 MeV distribution and three distinct lobes in the 4 MeV and 7 MeV distributions. The changing number of lobes shows the behavior is not just scaled based on energy, but can have distinct features appear and disappear along a given energy range. Another important feature to note is that at 1 MeV, there is no forward scatter or backscatter bias, but this is not true at higher energies.

The same plot in Figure 5 was repeated in Figure 6, only changing the species struck to N^{14}. Only elastic scatter is represented, and 1 MeV, 4 MeV, and 7 MeV are represented.

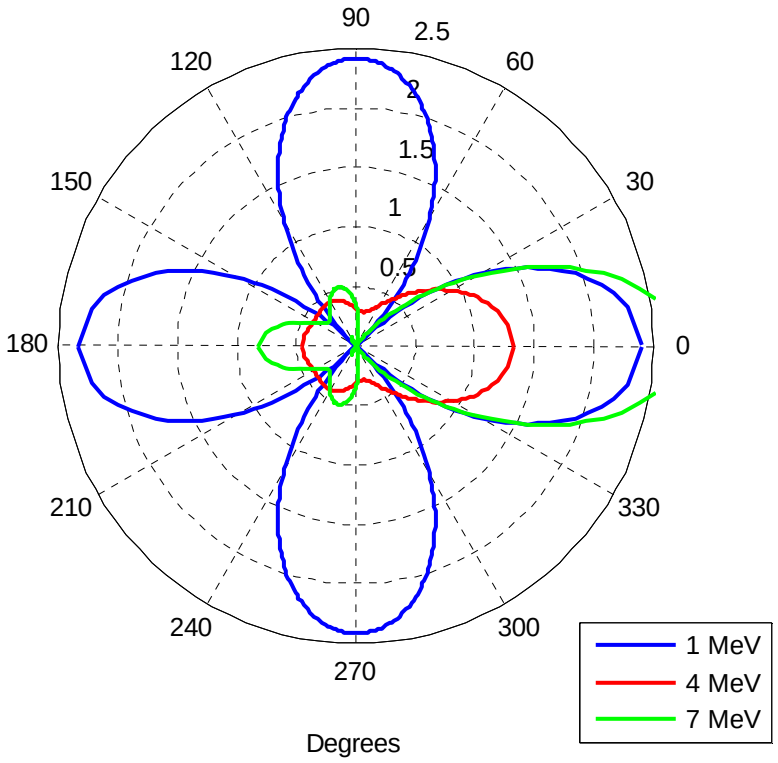

Figure 6: $f(\mu_{CM})$ plotted radially against $\theta(\mu_{CM})$ of Neutrons at 1 MeV, 4 MeV, and 7 MeV following elastic scattering events with N^{14}. These energies are measured in the reference frame of the center of mass of the collision. With changing energies of incident neutron colliding with the same species in only elastic scattering events, significantly different angular distributions result.

Similar to Figure 5, the 1 MeV distribution shows no forward or backscatter bias, but the forward scatter bias is clearly evident at higher energies. Again, the lobes of the distributions appear to present themselves and disappear as energy changes.

Once it was clear that anisotropic scatter is present across energy levels, inelastic level scatter was examined. Since it is now established that the anisotropic behavior can vary with energy, the next task would be to determine if anisotropic behavior varies with the level of an inelastic scatter.

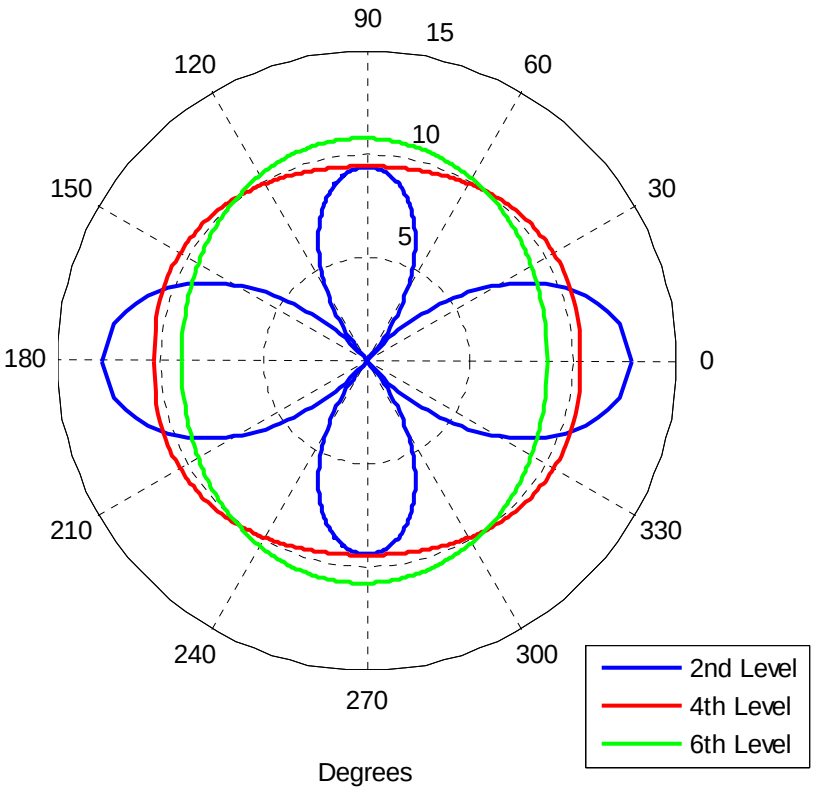

Figure 7: $f(\mu_{CM})$ plotted radially against $\theta(\mu_{CM})$ of 8 MeV Neutrons following 2^{nd}, 4^{th}, and 6^{th} level inelastic scattering events with O^{18}. These energies are measured in the reference frame of the center of mass of the collision. With the same energy of incident neutron colliding with the same species, based on the inelastic level, significantly different angular distributions result.

Figure 7 shows the angular distribution for varying levels of anisotropy across inelastic levels, where the angular distributions from three inelastic level scatters (2^{nd},

4^{th}, and 6^{th}) from 8 MeV neutrons are incident to O^{18}. Three distinct scattering behaviors are observed. First, in the 2^{nd} level inelastic scatter four lobes are present, indicating a forward scatter, backscatter, and direct side scatter bias with zeros between those lobes. Next, in the 4^{th} level inelastic scatter a slight forward scatter and backscatter bias is observed, with smooth transitions throughout. Finally, in the 6^{th} level inelastic scatter, a slight bias to side scatter is observed, again with smooth transitions.

Figures 5, 6 and 7 are not present to show patterns, or to draw definitive conclusions, but they do clearly show that anisotropic behavior is present, and that the behavior can vary across any of the parameters of the collision, namely species struck, inelastic level, and incident neutron energy. However, there is no expectation that a clear pattern would emerge. If there was a distinct pattern, a closed-form solution would likely be common practice for determining neutron scatter behavior.

Instead, the conclusion that can be drawn is that anisotropic behavior is clearly present in neutron scatter events, and bears investigation, as it may have significant effect on certain simulations related to long-distance, point source problems.

Weighted Random Choosing

Next, in order to verify both the cross section method for choosing collision types and the Watt spectrum for determining incident neutron energies, 100 million energies

were drawn from the Watt spectrum, and collisions types were tabulated using cross sections and atmospheric concentrations.

During this process of weighted random sampling, individual neutrons with their associated energies were examined, and virtually every possible collision type and species was encountered, ensuring that the chance of each type of collision was appropriately weighted as shown in Equation [3.1] and in Equation [3.2].

Table 1: Listing of Collisions Produced by 10^8 Neutrons Drawn from the Watt Spectrum. Atmospheric species fractions along with cross sections were used in weighting the collisions.

Level	$\mathbf{N^{14}}$	$\mathbf{N^{15}}$	$\mathbf{O^{16}}$	$\mathbf{O^{18}}$	$\mathbf{O^{17}}$
0	72886617	387202	25451238	7492	5388
1	213075	1142	13427	1529	629
2	439105	426	89258	186	41
3	76752	298	18133	132	77
4	165195	178	8093	331	27
5	43304	117	2775	144	11
6	74840	128	576	69	34
7	24413	21	484	76	12
8	11900	20	597	25	17
9	31891	5	307	64	0
10	8992	14	354	59	9
11	5236	21	295	20	3
12	9230	6	198	33	1
13	2761	7	243	31	2
14	251	5	9	3	4
15	181	7	4	8	2
16	227	4	10	2	2
17	1869	2	2	2	2
18	2817	5	2	2	3
19	2865	4	0	5	1
20	1836	0	0	6	2
21	728	0	0	3	1
22	1182	0	0	7	6
23	898	0	0	5	0
24	658	0	0	2	0
25	470	0	0	1	1
26	274	0	0	2	0
27	180	0	0	3	0
28	114	0	0	1	2
29	0	0	0	2	0
30	0	0	0	0	0

Table 1 functions as a display of the collision choosing portion of the module. Several elements of the table are present as expected, such as the majority of collisions are incident to N^{14}, the most plentiful species in the defined atmosphere. Additionally, the majority of the collisions are elastic (98.77%), represented by the 0^{th} level.

The Effect of Anisotropy

With the individual elements of the module functioning in accordance with theory, the underlying question is whether anisotropic behavior is worth the computational cost to be included in certain HASTE-N problem runs, and if so, what level of precision is effected by the inclusion of anisotropic scatter. The first part of this question is addressed here, and the latter will become apparent as the HASTE-N software package goes through further testing and development.

First, given the reasonable set of parameters for a sample problem listed in Table 2 (coefficients for the Watt spectrum representing neutrons emitted from the fission of U^{235}, and a five species atmosphere consisting of two isotopes of nitrogen and three isotopes of oxygen with associated concentrations), 10^8 collisions were selected by random sampling producing the collisions listed in Table 1.

Table 2: Problem Parameters

Atmospheric Fractions	
Nitrogen	0.78084
Oxygen	0.20946

Watt Spectrum Coefficients	
a	0.7
b	1

Isotopic Concentrations	
N14	0.99636
N15	0.00364
O16	0.99757
O18	0.00205
O17	0.00038

Next, the energy of each incident neutron causing each of the 10^8 events was used to determine the species struck and the inelastic level. This information was then used to interpolate tabulated Legendre coefficients. These 10^8 sets of coefficients were averaged, producing an average PDF of first scatters, $\tilde{\mathrm{f}}\left(\mu\right)$, for the problem as a whole, representing the overall scatter angle distribution for the problem parameters, taking into account weighting from collision type, incident energy, and species struck. This overall $\tilde{\mathrm{f}}\left(\mu\right)$ is graphed in Figure 8 below.

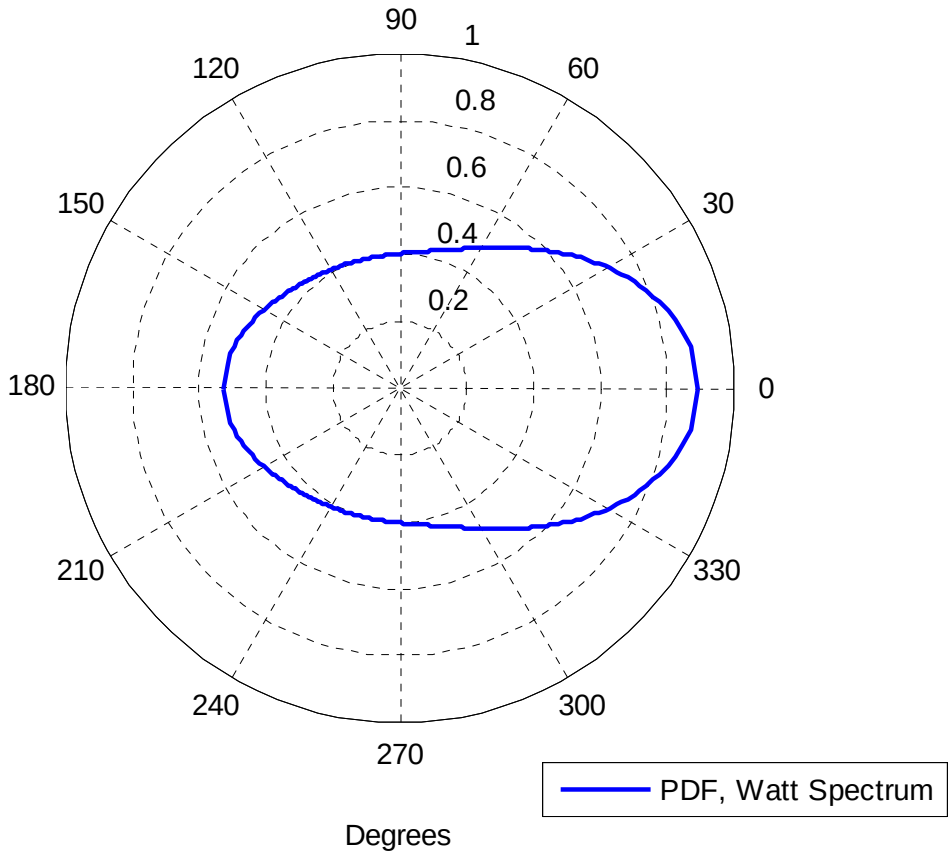

Figure 8: $f\left(\mu_{CM}\right)$ plotted radially against $\theta(\mu_{CM})$ of 10^8 neutrons drawn from the Watt spectrum for U^{235} fission incident to an atmosphere as specified in Table 2. The anisotropic nature of the angular distribution PDF is apparent, with a significant forward bias.

The overall $\tilde{\mathrm{f}}\left(\mu\right)$ does not have any distinct lobes or sharp features, as it is averaged over 10^8 different function estimators. Readily apparent is a forward bias, with a distinct bias for deflection angles less than 30 degrees. This shows that the problem set as a whole has significant anisotropic behavior and should be considered in problems with parameters similar to those in Table 2.

Because lower energies are shown to show less forward bias, as seen in Figure 5 and Figure 6, the same averaging was examined excluding lower energies. Considering this anisotropic behavior, excluding lower energies could be useful if a given detection system has a lower energy threshold, or if due to the geometry of the problem, which has not been considered here, lower energy neutrons need not be considered.

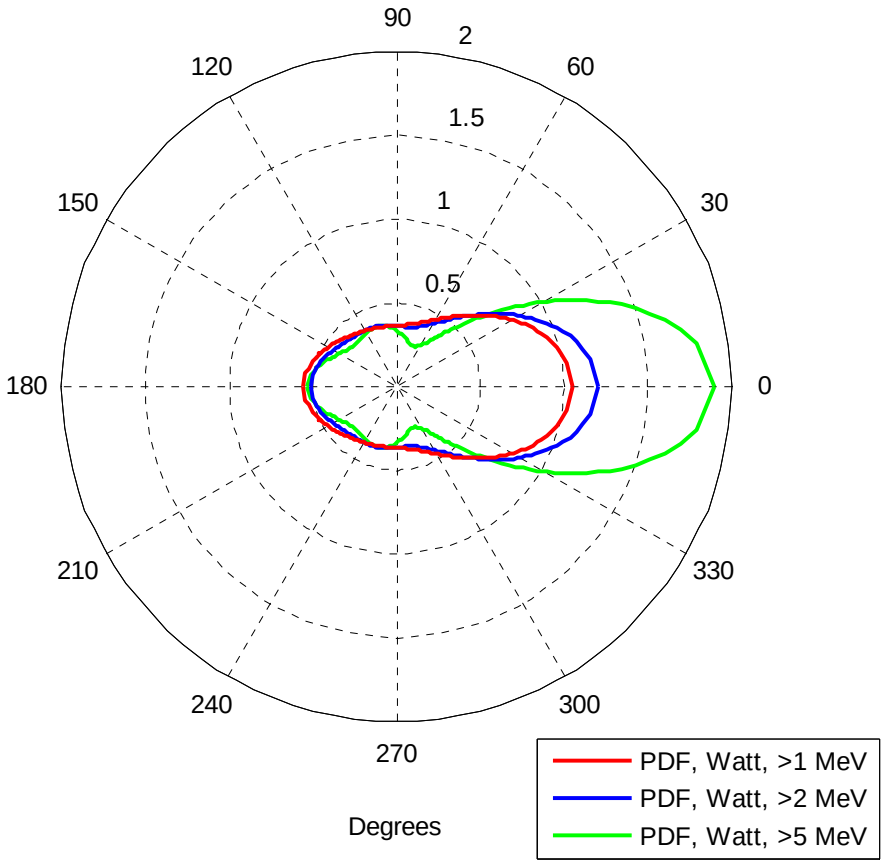

Figure 9: $f(\mu_{CM})$ plotted radially against $\theta(\mu_{CM})$ in varying energy ranges of 10^8 neutrons drawn from the Watt spectrum for U^{235} fission incident to an atmosphere as specified in Table 2. Distributions shown suppress lower energies. When higher energies are

displayed absent lower energies the foreword bias is more apparent, showing the forward bias comes from the higher energy neutrons more than the lower energy neutrons.

When the same 10^8 neutrons are considered, masking out lower energies, the foreword bias becomes more apparent. In fact, as a larger range of low energies is masked, as in Figure 9, bias is more prominent.

This leads to the conclusion that, on average, the higher the energy, the greater the apparent magnitude of the forward bias of the anisotropic scatter. Based on the design of the problem, including geometry and detector sensitivity, this further increased anisotropy of scatter angle could have an even greater effect on the fidelity of the model.

Altitude Parameter Study

Through the use of HASTE-N-TE, a study varying altitude while examining anisotropy was conducted. HASTE-N-TE was configured to utilize a 14.06 MeV isotropic line source, forcing a leakage-suppressed first elastic scatter only, and then populating energy-time bins through the use of a point estimator.

The atmosphere used in the study is of uniform density and is composed of isotopic concentrations listed in Table 2 and stretches from 0 to 86 km above the earth with vacuum above. The atmosphere is 1-D slab geometry, above a flat earth. The detector was placed at 30,000 km and the source location was varied in 5 km increments from 5 km to 85 km. Using these parameters, two runs of 10^8 particles at each altitude

were simulated, the first run using isotropic scatter, then the second using anisotropic scatter as determined by the scattering module.

Prior to examining any results, knowing the line source is 14.06 MeV and that nitrogen-14 is the most common species in the atmosphere, the anisotropic behavior of 14 MeV neutrons elastically scattered off nitrogen-14 was examined and is displayed in Figures 10 and 11 below.

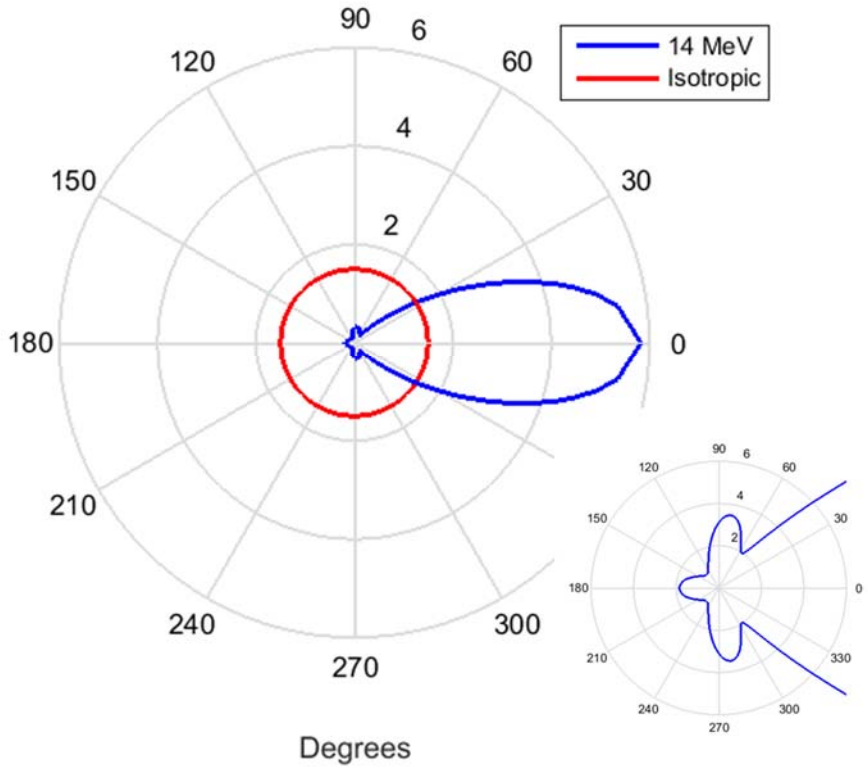

Figure 10: $f(\mu_{CM})$ plotted radially against $\theta(\mu_{CM})$ of 14 MeV neutrons following elastic scattering events with N^{14} including detail of side and backscatter regions. This distribution is measured in the reference frame of the center of mass of the collision and generated directly from ENDF coefficients. Scaled to arbitrary units of intensity.

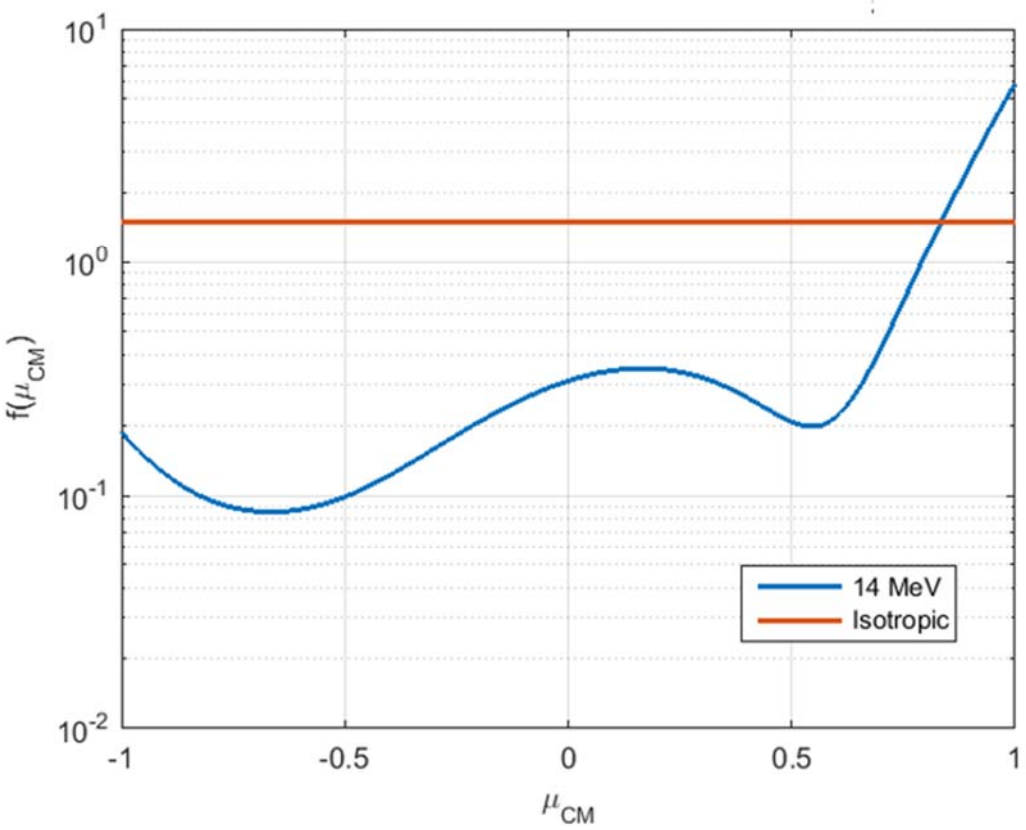

Figure 11: $f(\mu_{CM})$ plotted against μ_{CM} of 14 MeV neutrons following elastic scattering events with N^{14}, units of μ vs. arbitrary intensity units of the generated PDF, f(μ). This distribution is measured in the reference frame of the center of mass of the collision and generated directly from ENDF coefficients.

Examining Figures 10 and 11, a forward positive bias presents itself at scatter angles less than 27° with a negative bias present for side and back scatter regions. The uniform intensity of 0.5 representing isotropic, the point where the forward bias end can be determined by setting f(μ) equal to 0.5.

$$\begin{aligned} f(\mu) &= 0.5 \\ \mu &= \cos(27°) = 0.893 \end{aligned} \quad . \qquad [4.1]$$

Even though the lobes representing side scatter shown in Figure 10 are significantly less than isotropic, it should be noted that the center of a lobe in the polar plot of the distribution can be mathematically located by setting the derivative of f(μ) equal to zero.

$$\begin{aligned} f'(\mu) &= 0 \\ \mu &= \cos(85^\circ) = 0.087 \end{aligned} \quad . \qquad [4.2]$$

In order to examine the time-energy bins from each of the runs of this study, to best measure the relative effect of anisotropy, the time and energy dimensions were examined separately. First, neutron counts in time-integrated energy bins were plotted at varying altitudes, then neutron counts in energy-integrated time bins were plotted at the same varying altitudes. Collapsing these dimensions allows a good display of the relative difference of anisotropic scatter as compared to isotropic scatter in the time and energy dimensions.

Time-Integrated Energy Bins

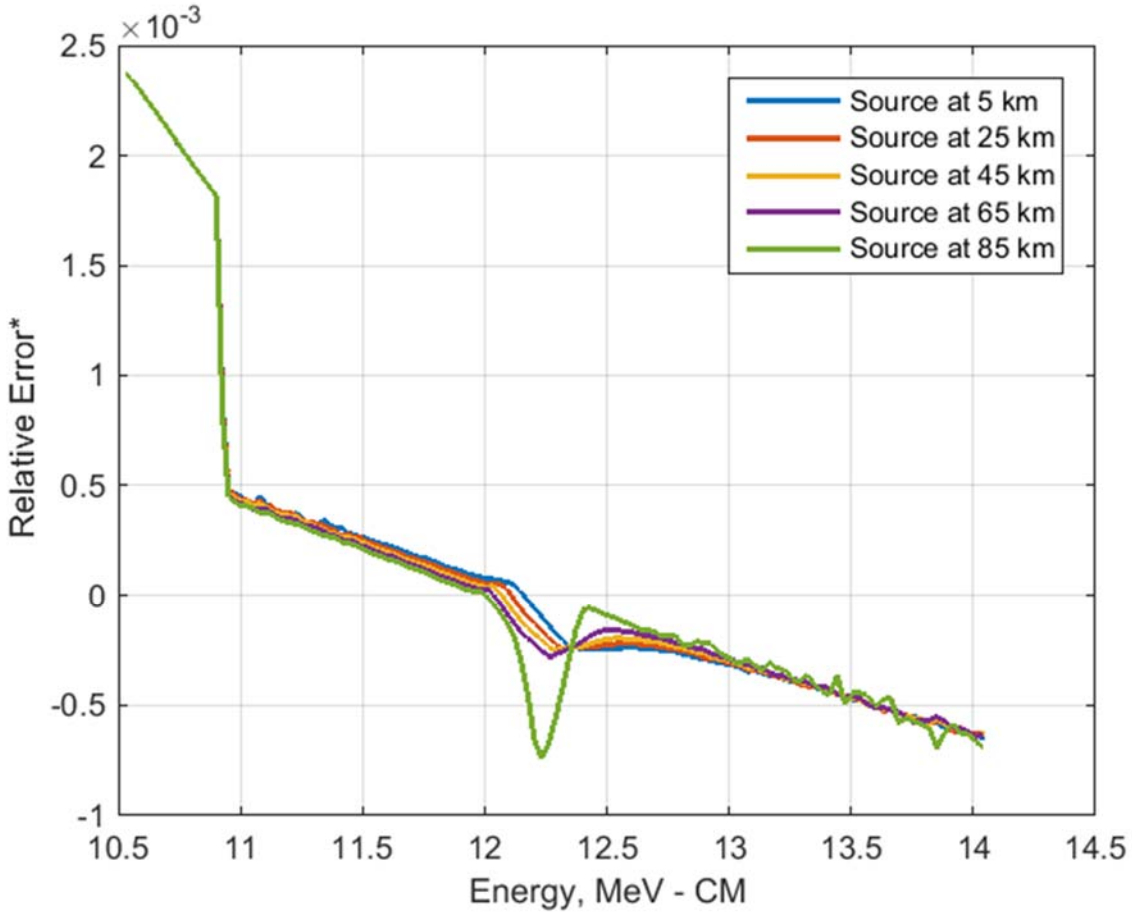

Figure 12: Energy bin neutron counts vs. relative error over five source altitudes. Relative error is calculated with anisotropic treated as the true value and isotropic treated as the measured value.

The relative error between neutron counts in isotropic and anisotropic time-integrated energy bins,

$$\varepsilon_{rel} = \frac{\varphi_{isotropic} - \varphi_{anisotropic}}{\varphi_{anisotropic}}, \qquad [4.3]$$

as shown in Figure 12, has several distinct features that are directly linked to anisotropic scatter behavior. Thus, where the relative error is positive, a calculation using isotropic scatter in the CM frame overestimates the result of a calculation that uses the ENDF anisotropic scatter in the CM frame.

First, in a direct backscatter collision event, where the neutron deposits the maximum amount of energy in the atom, and has minimal exit channel energy, the isotropic scatter model overestimates counts by nearly 0.24%. This occurs where the difference between the isotropic distribution and the anisotropic distribution of nitrogen-14 diverge the most, at a direct backscatter.

The maximum energy loss in a collision, $\Delta E_{loss} = E' - E$, for a 14 MeV neutron, $E' = 14 \text{ MeV}$, is

$$\Delta E_{\substack{\max \\ \text{loss}}} = E' \frac{4 m_n m_a}{\left(m_n + m_a\right)^2} = \left(14 \text{ MeV}\right) \frac{\left(4\right)\left(1\right)\left(14\right)}{\left(1+14\right)^2} \approx 3.5 \text{ MeV}, \qquad [4.4]$$

so that the minimum energy of the neutron after the backscatter $\mu_{cm} = -1$, is

$$\mathrm{E}_{\min} = 14 \text{ MeV} - \Delta E_{\substack{\max \\ \text{loss}}} \approx 10.5 \text{ MeV}. \qquad [4.5]$$

This is seen in Figure 12. It should be noted that in equation [4.4] the change in reference frame is not accounted for, as exit channel energy remains in the center of mass frame of the collision in this study.

Second, an analogous and opposite behavior presents itself in the region of forward scatter, where energy transfer is minimal, and exit channel energy is near 14 MeV. Here, an underestimate by isotropic scatter is evident, a result of the distinct forward bias of nitrogen-14 anisotropic scatter in the forward region, as seen in Figure 10.

The dip in the center of the graph in Figure 12 is a combination of both the design parameters of the simulation, and of the sideways scatter bias of oxygen-16, the second most common species in the defined atmosphere. Here, due to the 1-D slab geometry and flat earth model used, some neutrons travel nearly parallel to the top of the atmosphere for a long distance before scattering, then, the point estimator only attenuates the neutron slightly before it exits the atmosphere and is tallied. This is more pronounced at higher source elevations, as the source is closer to the top of the defined atmosphere. Oxygen-16 exhibits an elastic side scatter bias at higher energies, which is why the isotropic scatter model is an underestimate.

At the highest source elevation, 85 km, some noise is present at the higher energy bins, or the bins populated by forward scatter events because the scatter is forced to

occur in a small amount of the atmosphere, and when assigned the correspondingly low weight using Monte-Carlo methods, produces poor counting statistics.

Energy-Integrated Time Bins

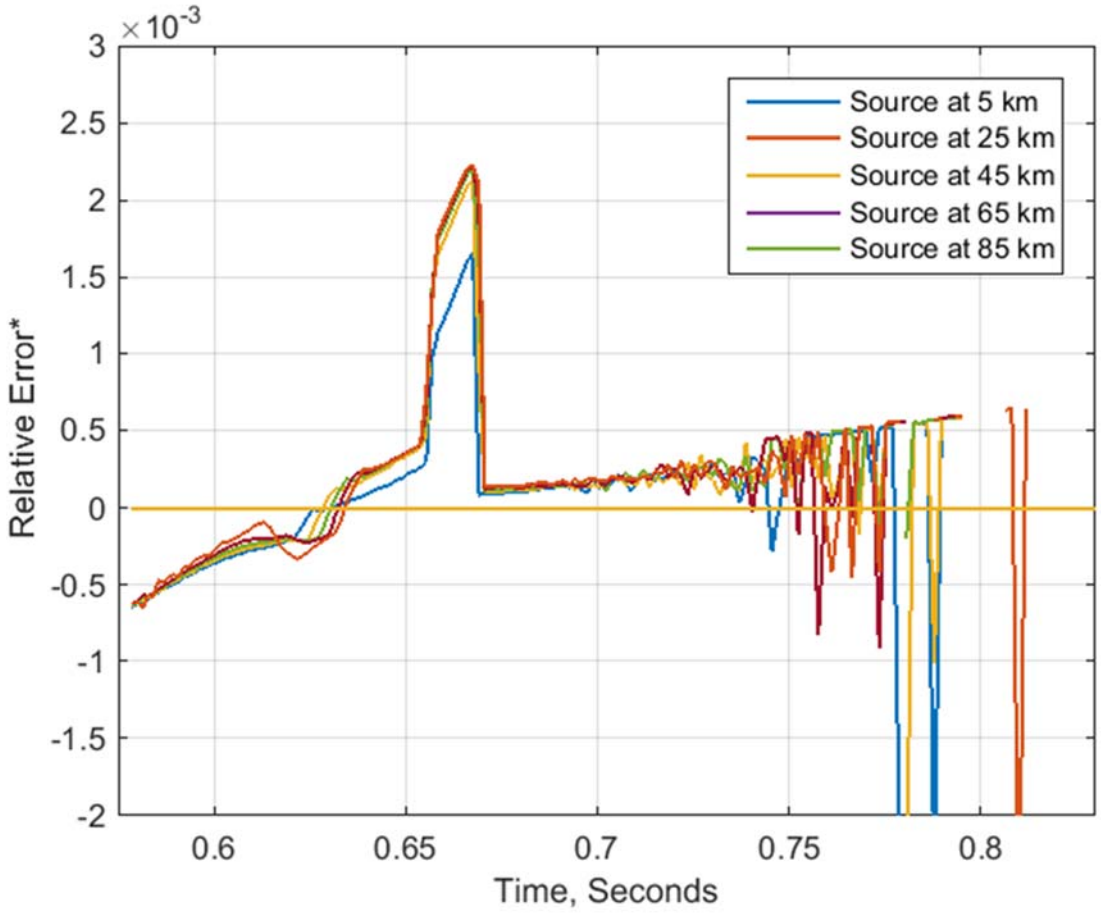

Figure 13: Time bins neutron counts vs. relative error over five source altitudes. Relative error is calculated with anisotropic treated as the true value and isotropic treated as the measured value.

Now, examining the same time-energy bin relative error data as in Figure 12, but with energy-integrated energy bins shown in Figure 13, several additional features can

be noted. First, the relative error is zero in figure 13, between 0.625 and 0.64 seconds depending on source altitude. This corresponds to a scattering angle of 27°. At this angle, the anisotropic angular distribution for nitrogen-14 intersects with the isotropic distribution case, as seen in Figure 10. This behavior is expected, at the angle where an anisotropic scatter distribution matches the value of an isotropic distribution the error between the two would be zero, and the expected difference of the time-energy bins populated by that particular scatter should also be near zero.

Second, at ~0.66 seconds, a significant peak in the error is present, getting larger at higher source altitudes. This phenomena is a direct result of the negative bias toward backscatter of nitrogen-14. The isotropic scatter model significantly overestimates the weight of a particle going down into the atmosphere from the source then backscattering to the detector. It follows that, for a higher source location, there is more atmosphere to travel through, and hence the collision is given a higher weight, leading to increased relative error with increasing source altitudes. This leads to a maximum of 0.23% relative error.

Finally, at times past 0.7 seconds, a significant increase in noise is present and is not consistent with increasing altitudes. This is primarily an artifact of the 1-D slab geometry combined with the backscatter mechanics of nitrogen-14 and oxygen-16.

One way to achieve a flight time of 0.75 seconds is as follows,

$$\sqrt{\frac{2(14\text{MeV})}{m_n}}\left(0.75-t\right)=d_1,\sqrt{\frac{2(10.5\text{MeV})}{m_n}}\left(t\right)=d_2$$
$$d_1{}^2+d_2{}^2=\sim 30000^2$$
$$t=0.71\,\text{sec} \qquad [4.6]$$
$$d_1=1446\text{km}$$
$$d_2=29965\text{km}$$

where d_1 is the distance traveled prior to the scatter, and d_2 is the distance between the scatter and the detector. Here, the neutron travels nearly parallel to the flat earth for 1446 km and then up to the detector. This is only possible with a 1-D slab geometry flat earth model. Since scattering events similar to the example have an extremely low weight due to the long distance traveled within the atmosphere, they produce poor counting statistics, hence the noise.

The noise, however, is not consistently positive or negative relative error. This is as a result of the species struck. Nitrogen-14, the most common species struck in the atmosphere, has a negative side-scatter bias and oxygen-16, the second most common species, has a positive side-scatter bias. This, combined with poor counting statistics means single events have a significant effect on the noise depending on the species struck, nitrogen-14 showing isotropic producing an overestimate, and oxygen-16 producing an underestimate for the scattering events that populate time bins in this region.

Energy Parameter Study

Through the use of HASTE-N-TE, a study varying energy while examining anisotropy was conducted. HASTE-N-TE was configured to utilize 11 isotropic line source energies ranging from 1 MeV to 14 MeV, forcing a leakage-suppressed first elastic scatter only, and then populating energy-time bins through the use of a point estimator.

The atmosphere used in the study is of uniform density and is composed of isotopic concentrations listed in table 2 and stretches from 0 to 86 km above the earth with vacuum above. The atmosphere is 1-D slab geometry, above a flat earth. This configuration is identical to that used in the altitude parameter study.

The detector was placed at 30,000 km and the source location was fixed at 43 km, the center of the defined atmosphere. Using these parameters, two runs of 10^8 particles at each energy were simulated, the first run using isotropic scatter, then the second using anisotropic scatter as determined by the scattering module.

Since flight times vary both with the scatter mechanics and the energy of the line source, the results of this study are best viewed in the relative error of time-integrated energy bins. This allows analysis of the change in the shape of the relative error vs. energy plot shown in Figure 14 as incident energy varies.

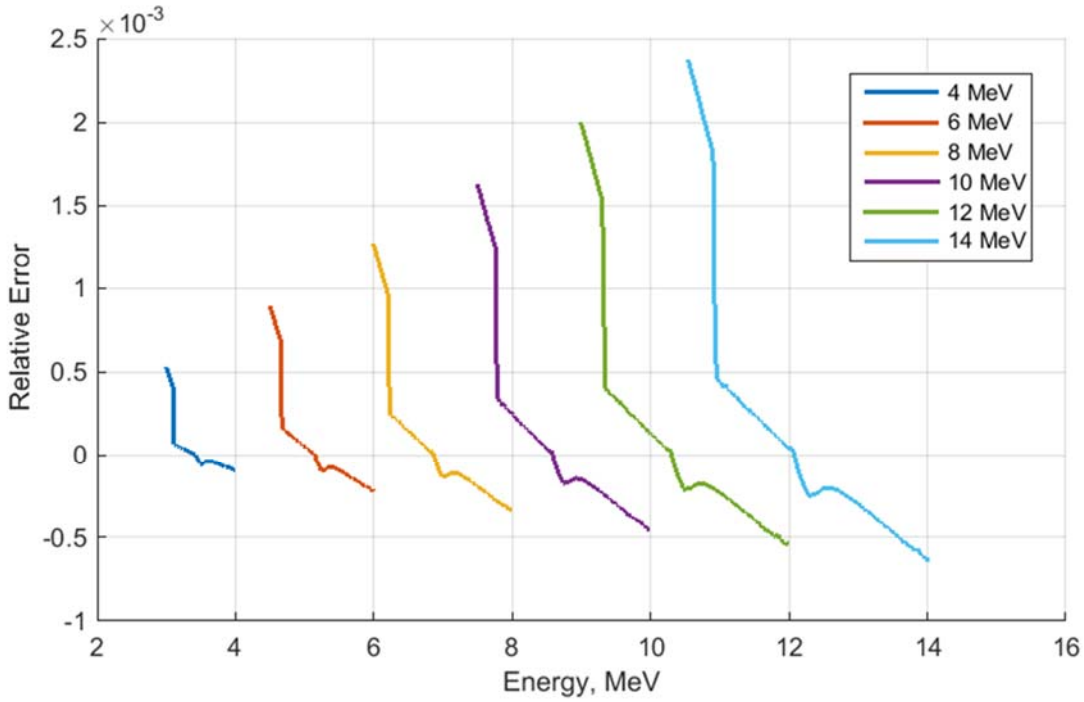

Figure 14: Energy vs. relative error, energy varying from 4 MeV to 14 MeV. Relative error is calculated with anisotropic treated as the correct value and isotropic treated as the approximate value.

In the energy range depicted in Figure 14, the shape of each relative error vs. energy plot is similar to that seen in Figure 12, with the same interpretation for the features in each plot as described in the altitude study. Primarily, this is evidence that the behavior of the relative error of time-integrated energy bins is consistent across an energy range, not just at 14.06 MeV as analyzed in the altitude study.

Additionally, across the energy range of 4 MeV to 14 MeV as displayed in Figure 14, the relative error increases linearly with energy. This behavior of the relative error

can be used as a determining factor when deciding to apply anisotropy to an energy range, based on the noise level of a particular simulation or the precision desired.

At energies beneath 4 MeV, however, the shape of the relative error plot begins to change as seen in Figure 15. The maximal error shifts from the left of each plot, meaning the region of energy bins populated by backscatters, to the right side of the plots, the region of energy bins populated by the forward scatters.

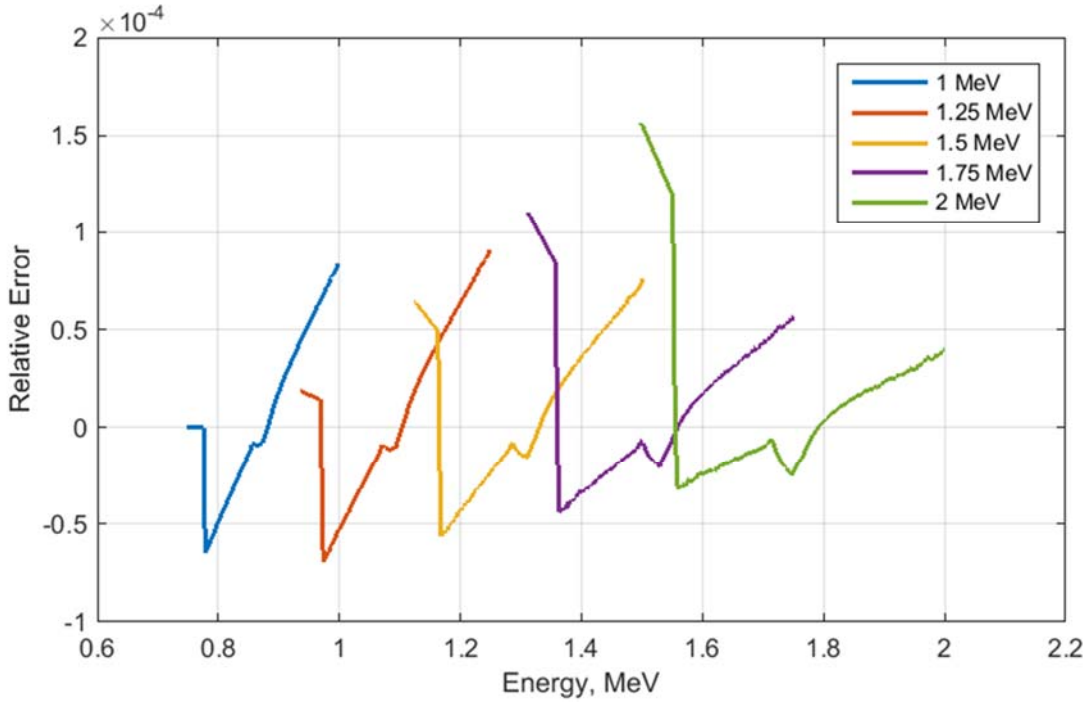

Figure 15: Energy vs. relative error, energy varying from 1 MeV to 2 MeV. Relative error is calculated with anisotropic treated as the correct value and isotropic treated as the approximate value.

Due to the decreasing relative error in the 1 MeV to 2 MeV energy range combined with the effect of anisotropy being reduced for this energy range as seen in

Figure 6, the artifacts of the problem parameters may eclipse any conclusions that could be drawn from this behavior. Higher fidelity simulation in HASTE-N focused on this energy range could allow more definitive conclusions regarding the behavior of the relative error in this energy region.

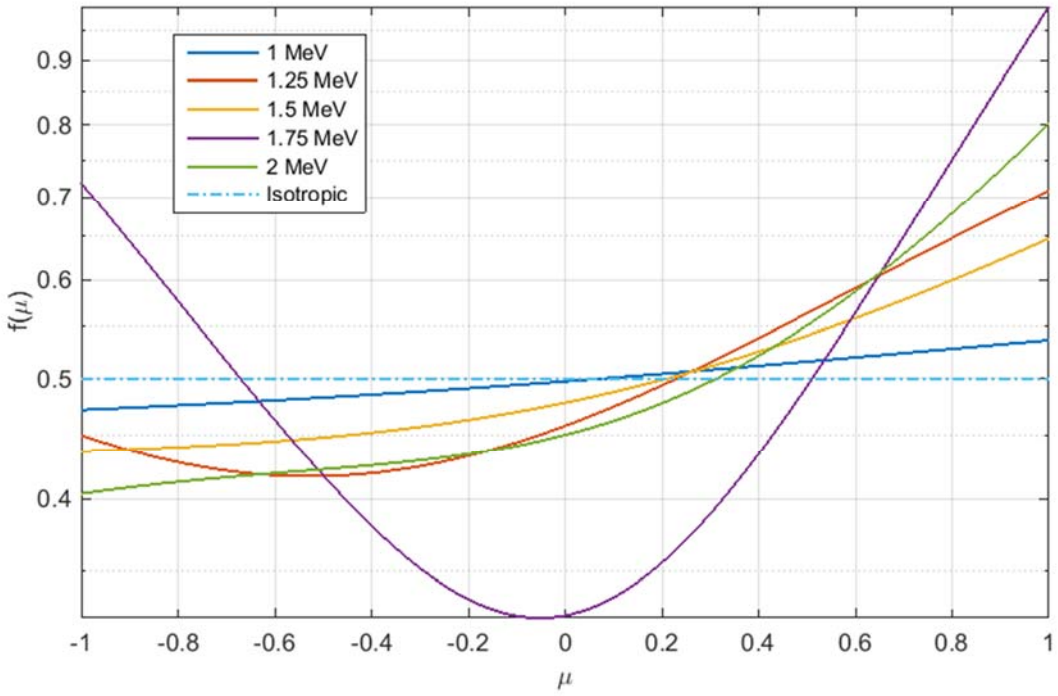

Figure 16: Probability density functions for elastic scattering of nitrogen-14, 1 MeV to 2 MeV. Plot is of μ vs. normalized intensity of each PDF. Legendre coefficients are extracted from ENDF without interpolation.

The behavior of the angular distribution probability density functions for nitrogen-14, as shown in Figure 16, shows oscillations in the behavior of the PDFs that are not easily explained. This does not clearly explain the behavior of the relative error of energy bins in this region, leading to the supposition that the shift in the shape of the

relative error plots in Figure 15 is not related to anisotropic behavior changes, but from a different aspect of the simulation.

V. Conclusion

Anisotropy is present in the angular distributions of neutrons departing from a nuclear scattering event. This anisotropy cannot be defined in a closed-form solution as in the Klien-Nishina distribution for gamma rays following scattering events, nor is the degree and behavior of anisotropy only dependent on the incident energy of the particle. In fact, for neutrons leaving a scattering event, the anisotropic behavior of the angular distribution is dependent on the incident energy of the neutron, the type of scatter being elastic or inelastic along with the inelastic level, and the species struck. Additionally, this dependence cannot be predicted using a closed form solution, and polynomial functions have been developed and are tabulated in ENDF based on experimental data.

The function used to describe the estimator of the PDF of the angular distribution for a given set of conditions is constructed of weighted Legendre polynomials. In general, the larger the magnitude of the weighting coefficients, the more severe the anisotropy. Unfortunately the shape of the angular distribution is not predictable based on any consistent factor, and experimental data must be used to construct angular distributions for use in simulation models.

Amidst all of the other computational demanding factors of a Monte Carlo neutron transport code including problem geometry, fidelity demands, cross section lookups, and others, inclusion of anisotropic scattering behavior requires examination to

determine if the increase in computational cost adds appreciably to the fidelity of the answer, and to what degree fidelity is increased.

A spectrum of U^{235} fission neutrons, as generated by the Watt spectrum, was examined as it collided with species in a nitrogen-oxygen atmosphere with normal natural concentrations of nitrogen and oxygen isotopes. In a stochastic manner, 10^8 collision samples were taken, utilizing cross section-based weighting for random sampling of collision types and cross section weighting along with concentration weighting to determine the species struck. The collective anisotropy of the resultant angular distribution was apparent, with a definite average forward bias across the spectrum and a bias toward scattering angles less than 30 degrees.

Additionally, when lower energies are eliminated from consideration, the forward bias increases. This leads to the conclusion that, on average, the higher the energy, the greater the apparent magnitude of the forward bias of the anisotropic scatter. This is worth considering when undertaking simulation design utilizing detectors with specified sensitivity ranges.

Using 1-D slab geometry, two studies were conducted exploring the relative effect of anisotropic scatter as compared to isotropic scatter in the center of mass reference frame. The maximum relative error of 0.24% was observed in the energy dimension and 0.23% in the time dimension. This can serve as a first approximation for more complex problem geometries and more robust scatter mechanics. In short, if precision is required

past the second decimal place in long-distance high-altitude transport utilizing isotropic scatter in the center of mass reference frame, anisotropy in the center of mass reference frame deserves consideration.

Further Work

Additional examination regarding the specific nature of the anisotropy is suggested, particularly within a simulation. Once HASTE-N is able to function with and without implementation on anisotropic scatter, detailed parameter studies should be conducted to determine the gain in fidelity realized by the inclusion of anisotropic neutron scatter.

Bibliography

[1] Mathews, Kirk A. "HASTE-N High Altitude / Space Transport Estimator for Neutrons: A Monte Carlo Method for Neutron Transport Within and Above the Atmosphere to a Satellite-Based Detector." Unpublished, January 2015

[2] Lewis, E.E. and Miller, W.F. Jr. *Computational Methods of Neutron Transport*. La Grange Park, IL: American Nuclear Society, 1993.

[3] Mathews, Kirk A. Professor of Nuclear Engineering, School of Engineering and Management, Air Force Institute of Technology, Wright-Patterson AFB OH, Personal Correspondance, Fall Quarter 2014.

[4] Lawrence Livermore National Laboratory. Sampling ENDL Watt Fission Spectra. UCRL-TR-203351. Livermore CA: LLNL, 1 April 2004

[5] Lawrence Livermore National Laboratory, *The LLL Evaluated Nuclear Data Library (ENDL): Evaluation Techniques, Reaction Index, and Description of Individual Evaluations*. UCRL-50400, Vol. 15, Part A, Livermore, CA: LLNL, September 1975

[6] Brookhaven National Labratory, *ENDF-6 Formats Manual: Data Formats and Procedures for the Evaluated Nuclear Data Files ENDF/B-VI and ENDF/B-VII*. BNL-90365-2009, Revision 2. Upton, NY: BNL, December 2011

[7] *Microsoft Visual Studio Professional 2013*, Version 12.0.30501.00 Update 2. Computer Software. Microsoft Corporation, Redmond, WA, 2013.

[8] *MatLab 2014b*, Version 8.4.0.150421. Computer Software. The Mathworks Inc, Natick MA, 2015.

REPORT DOCUMENTATION PAGE

Form Approved
OMB No. 0704-0188

PLEASE DO NOT RETURN YOUR FORM TO THE ABOVE ADDRESS.

1. REPORT DATE *(DD-MM-YYYY)*	2. REPORT TYPE	3. DATES COVERED *(From - To)*
26 Mar 2015	Master's Thesis	June 2013 - March 2015

4. TITLE AND SUBTITLE

The Effect of Anisotropic Scatter on Atmospheric Neutron Transport

5a. CONTRACT NUMBER

5b. GRANT NUMBER

5c. PROGRAM ELEMENT NUMBER

6. AUTHOR(S)

McIntee, Nicholas, J, Major, United States Army

5d. PROJECT NUMBER

5e. TASK NUMBER

5f. WORK UNIT NUMBER

7. PERFORMING ORGANIZATION NAME(S) AND ADDRESS(ES)

Air Force Institute of Technology
Graduate School of Engineering and Management (AFIT/EN)
2950 Hobson Way
Wright-Patterson AFB OH 45433-7765

8. PERFORMING ORGANIZATION REPORT NUMBER

AFIT-ENP-MS-15-M-085

9. SPONSORING/MONITORING AGENCY NAME(S) AND ADDRESS(ES)

Air Force Technical Applications Center
Dr. David Walter Gerts
10989 South Patrick Dr.
Patrick AFB, FL 32925
david.gerts.2@us.af.mil

10. SPONSOR/MONITOR'S ACRONYM(S)

AFTAC

11. SPONSOR/MONITOR'S REPORT NUMBER(S)

12. DISTRIBUTION/AVAILABILITY STATEMENT

Distribution Statement A. Approved for Public Release; Distribution Unlimited.

13. SUPPLEMENTARY NOTES

14. ABSTRACT

Anisotropy is present in the angular distributions of neutrons departing from a nuclear scattering event. This anisotropy cannot be defined in a closed-form solution, and it is dependent on the incident neutron energy, elastic or inelastic scatter, along with the inelastic level, and the species struck. The underlying question is, if anisotropic behavior is worth the computational cost to be included in certain simulations, and if so, what level of precision is effected by the inclusion of anisotropic scatter.

A Watt spectrum of U235 fission neutrons was examined as it collided with species in a nitrogen-oxygen atmosphere. The collective anisotropy of the resultant angular distribution was apparent, with a definite average forward bias across the spectrum and a bias toward scattering angles less than 30 degrees. Additionally, with the elimination of lower energies, on average, the higher the energy, the greater the apparent magnitude of the forward bias of the anisotropic scatter.

Using 1-D slab geometry, two studies exploring the relative effect of anisotropy were conducted. The maximum relative error of 0.24% was observed in energy and 0.23% in time. In short, if precision is required past the second decimal place in long distance

15. SUBJECT TERMS

Neutron Scatter, Anisotropy, Atmospheric Transport, Monte-Carlo

16. SECURITY CLASSIFICATION OF:			17. LIMITATION OF ABSTRACT	18. NUMBER OF PAGES	19a. NAME OF RESPONSIBLE PERSON
a. REPORT	b. ABSTRACT	c. THIS PAGE			Dr. Kirk A. Mathews
U	U	U	UU	73	19b. TELEPHONE NUMBER *(Include area code)* (937) 255-3636 x4508 kirk.mathews@afit.edu

Reset